

Supplementary Information

**Copper-palladium core-shell as anode in a multi-fuel
membraneless nanofluidic fuel cell: toward a new era of small
energy conversion devices**

J. Maya-Cornejo^a, E. Ortiz-Ortega^b, L. Álvarez-Contreras,^c N. Arjona^{a**}, M. Guerra-Balcázar^b, J. Ledesma-García^b, and
L.G. Arriaga^{a*}

^a Centro de Investigación y Desarrollo Tecnológico en Electroquímica, 76703 Querétaro, México. * E-mail:

larriaga@cideteq.mx **E-mail: noe.arjona@yahoo.com.mx

^b División de Investigación y Posgrado, Facultad de Ingeniería, Universidad Autónoma de Querétaro, 76010 Querétaro,
México

^c Centro de Investigación en Materiales Avanzados S. C., 31109 Chihuahua, Mexico.

1. Synthesis of Cu@Pd core-shell electrocatalyst

For the chemical synthesis of Cu@Pd core-shell, 0.1 g polyvinylpyrrolidone (PVP, wt. 40,000, Sigma-Aldrich), was used as surfactant, and 0.66 g ascorbic acid (99.0%, Sigma-Aldrich), employed as the reducing agent. These reagents were placed in a round-bottom flask containing 10 mL ethylene glycol (J.T. Baker, 99.92%) as reaction media and the flask was heated to 80 °C. After that, Cu salt (0.06 g CuSO₄, reagent grade, Sigma-Aldrich) was added to the solution, which was then stirred for 30 min to form the core of the electrocatalyst particles. Next, 0.25 g sodium bromide (NaBr, 99.0%, J. T. Baker) was added as additive to the mixture followed by 0.028 g potassium tetrachloropalladate (II) as the Pd²⁺ ion source (K₂PdCl₄, 99%, Aldrich). CuSO₄, NaBr and K₂PdCl₄ were each dissolved in 1 mL water before being added to the ethylene glycol solution, resulting in a total solution volume of 13 mL. The mixture was then stirred for 90 min to ensure complete reaction. Vulcan XC-72 carbon support (CABOT) was then added to the solution, and stirring was continued for another 30 min. The solution was washed several times with deionized water and dried overnight. The final metal mixture/support composition was 30/70 mass %. This composition was chosen to match the Pd loadings of the commercial Pt/C (Etek, 30 wt. %) and Pd/C (Etek, 30 wt. %) catalysts.

2. Electrochemical characterization

Cu@Pd/C core-shell and Pd/C electrocatalysts were evaluated by cyclic voltammetry in acidic media (0.5 M H₂SO₄), as shown in Fig. S1-a, and in alkaline media (0.3 M KOH), as observed in Fig. S1-b. In Figure S1-a, an electrochemical response typical of Pd-based materials was observed, where the hydrogen adsorption/desorption region occurred between 0 and 0.3 V vs. NHE. The formation of Pd oxides was observed in the region between 0.7 and 1.3 V vs. NHE, and the reduction of the Pd oxides occurred at 0.7 V vs. NHE.¹ The voltammogram of the Cu@Pd electrocatalyst contains several additional peaks: one observed in the positive sweep at 0.57 V vs. NHE is related to the formation of Cu oxides,^{2, 3} and the second peak, found in the negative sweep at 0.4 V vs. NHE, is related to the reduction of Cu oxides. These peaks corroborate the presence of Cu in the Cu@Pd electrocatalyst.

The cyclic voltammograms showed in Fig. S1-b also exhibited the typical electrochemical profile of Pd-based electrocatalysts. A peak in the anodic sweep was observed at -0.05 V vs. NHE and is associated with the formation of Pd oxides; the peak in the cathodic sweep between -0.16 and -0.02 V vs. NHE is related to the reduction of Pd oxides. A second peak in the anodic sweep, located at 0.19 V vs. NHE, is attributed to the oxidation of Cu in the Cu@Pd electrocatalyst.⁴ The cyclic voltammograms of the Cu@Pd/C and Pd/C electrocatalysts in alkaline media were used to calculate the electrochemically active surface area (ECSA) assuming the theoretical charge of 405 $\mu\text{C cm}^{-2}$ is required to reduce a full monolayer of Pd oxides.⁵ ECSAs of 14.049 and 2.756 cm^2 were calculated for the Pd/C and Cu@Pd/C electrocatalysts, respectively.

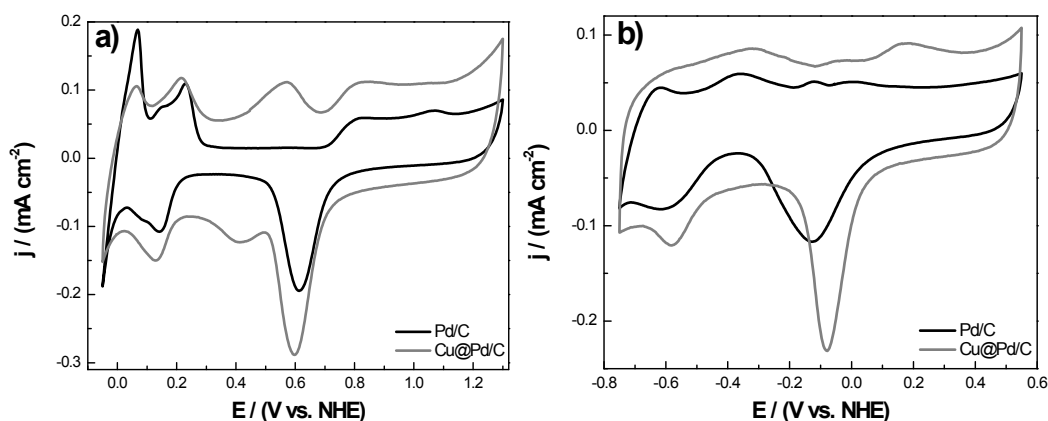


Figure S1. Cyclic voltammograms in a) acid media (0.5 M H₂SO₄) and b) basic media (0.3 M KOH) for Cu@Pd/C and Pd/C

The effect of the fuel concentrations was evaluated by cyclic voltammetry and the results for glycerol and ethylene glycol was showed in figure S2. Meanwhile, Table S1 gives a summary of the peak current densities for the electrooxidation of each of the fuels at a variety of fuel concentrations over both Cu@Pd/C and Pd/C. The Cu@Pd/C electrocatalyst yielded the highest values of current densities for ethanol and glycerol when the fuel concentration was increased to 3 M, generating densities higher by 4-fold with glycerol and 2-fold with ethanol compared to those produced by the commercial Pd/C electrocatalyst. This behavior arises from an enhancement in the electronic properties related with the interaction between noble/transition in the Cu@Pd electrocatalyst, which is in turn cause an electron rearrangement in the electronic structure due to a shifting on the central d-band (band narrowing). The electronic changes in the metal particles manifest as a modification of the surface properties of the Cu@Pd/C electrocatalyst, decreasing its binding energy.^{6, 7} Additionally, it is important to note that the Pd mass content in the Cu@Pd electrocatalyst was 40% less than commercial Pd/C.

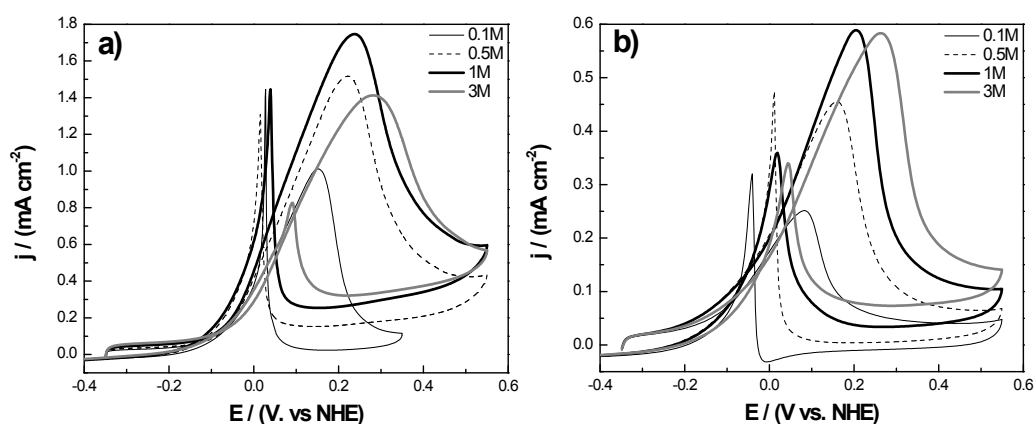


Figure S2. Electrocatalytic activity of Cu@Pd/C for a) glycerol and b) ethylene glycol conversion as a function of fuel concentration

Table S1. Peak current densities for Cu@Pd/C and Pd/C as a function of the fuel and its concentration

Concentration (M)	Catalyst	Current density (mA cm ⁻²)			
		Ethanol	Methanol	Ethylene glycol	Glycerol
0.1	Pd/C	0.13	0.13	0.27	0.28
	Cu@Pd/C	0.31	0.06	0.25	1.01
0.5	Pd/C	0.23	0.22	0.41	0.33
	Cu@Pd/C	0.54	0.13	0.46	1.52
1	Pd/C	0.36	0.26	0.41	0.36
	Cu@Pd/C	0.72	0.17	0.59	1.75
3	Pd/C	0.55	0.32	0.33	0.29
	Cu@Pd/C	1.40	0.24	0.58	1.41

3. Fabrication and operation of the membraneless nanofluidic fuel cell.

The cell components are shown in Fig. S3. This cell design is based on a previously reported, however some changes were made.⁸ It is shown in this figure that plates (S3a and S3d) for the fuel cell device were constructed of poly-(methyl-methacrylate) (PMMA), and the inlets, outlets and screw holes were made using a computer numerical control (CNC homemade 2.5 axis operated by Mach3 CNC Control Software). The window for air-breathing was placed in the top plate as well as the inlets for the different fuels (Fig. S3d). A silicone elastomer film (300 μm thick, Silastic® Dow Corning, Fig. S3b) was made and cut using a Silhouette® cutting plotter. The polymer film was placed along with the electrodes (Marketech, Inc.) between the plates (Fig. S3c) and served not only to seal the cell but also to orient the inlet solutions and the by-products towards the outlet (placed in Fig. S3a).

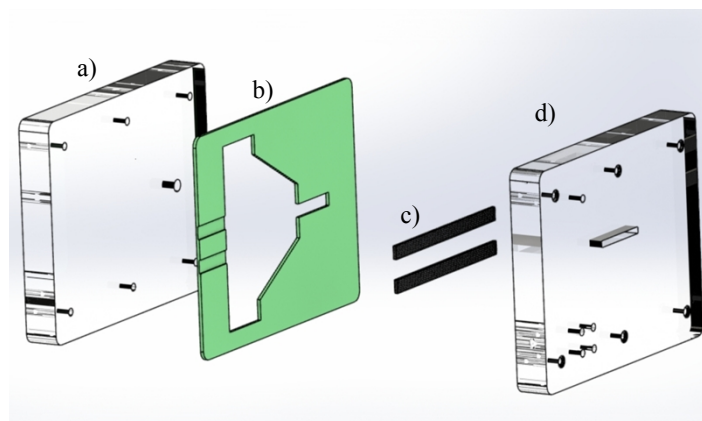


Figure S3. Components of the membraneless air-breathing nanofluidic fuel cell

The flow rates used in the air-breathing nanofluidic fuel cell changed as a function of the fuel due to the differences in their densities and viscosities. The flow rates were varied to find the optimal values presented in Table S2. The flows were pressure-driven using five syringe pumps, four being used to inject the fuels (Cole Parmer, single-syringe infusion pump, 115 VAC) and one for introducing the oxidant (Harvard Apparatus, PHD Ultra Syringe Pump Infuse/Withdraw). The fuels were tested by the following procedure: first, ethanol was injected into the nanofluidic fuel cell, the cell performance was tested, and a stability curve at high power density and high current density was evaluated for 30 minutes. After that, the ethanol flow was stopped, and the methanol solution was streamed for 5 minutes before starting the cell evaluation to ensure that the cell was free of ethanol, before again testing the cell performance and stability. This procedure was repeated for testing ethylene glycol, glycerol and the fuel mixture.

The values of power densities presented in Fig. 3 were compared with membraneless microfluidic fuel cells reported in literature which employs the fuels here presented using alkaline electrolytes and dissolved oxygen or air as oxygen source (Table S3).

Table S2 Optimal flow rates used for the different fuels in the air-breathing nanofluidic fuel cell

Fuel	Flow rate (mL hr ⁻¹)	Electrolyte	Oxidant	Flow rate (mL hr ⁻¹)
Ethanol	6	KOH 0.3M	Air + Oxygen (aq: sat.)	3
Methanol	12	KOH 0.3M	Air + Oxygen (aq: sat.)	12
Ethylene glycol	3	KOH 0.3M	Air + Oxygen (aq: sat.)	6
Glycerol	6	KOH 0.3M	Air + Oxygen (aq: sat.)	4
Multi-fuel mixture	6	KOH 0.3M	Air + Oxygen (aq: sat.)	3

Table S3 Comparison of cell voltages, current densities and power densities

	Anode	Fuel	Oxidant	Device	Cell voltage (V)	j (mA cm ⁻²)	P (mW cm ⁻²)
This work	Cu@Pd/C	Ethanol 0.1M	Air + Oxygen (aq: sat.)	AB-NFC	0.670	153.70	25.75
This work	Cu@Pd/C	Methanol 0.1M	Air + Oxygen (aq: sat.)	AB-NFC	0.621	100	17.1
Jayashree et al. ⁹	Pt/Ru	Methanol 1M	Air	AB- μ FC	1.05	120	17
This work	Cu@Pd/C	Ethylene glycol 0.1M	Air + Oxygen (aq: sat.)	AB-NFC	0.652	142.55	19.95
Arjona et al. ¹⁰	AuPd/ polyaniline	Ethylene glycol 2 M	Oxygen (aq: sat.)	μ FC	0.53	6.3	1.6
This work	Cu@Pd/C	Glycerol 0.1M	Air + Oxygen (aq: sat.)	AB-NFC	0.622	111.95	20.43
A. Dector et al. ¹¹	Pd/MWCNT	Glycerol 0.1M	Oxygen (aq: sat.)	μ FC	0.55	5	0.7
This work	Cu@Pd/C	Multi-fuel 0.1M	Air + Oxygen (aq: sat.)	AB-NFC	0.612	108.67	18.0

It is observed from Table S3 that exists few works in which the fuels here presented are successfully used in this kind of devices. The cell performances obtained through the use of the membraneless air-breathing nanofluidic fuel cell are the highest compared with those found in literature. Where for glycerol, the power density was increased almost 30-fold compared with the value reported by Dector et al.¹¹

References

1. N. Arjona, M. Guerra-Balcázar, F. M. Cuevas-Muñiz, L. Álvarez-Contreras, J. Ledesma-García and L. G. Arriaga, *RSC Adv.*, 2013, **3**, 15727-15733.
2. C. Xu, A. Liu, H. Qiu and Y. Liu, *Electrochem. Commun.*, 2011, **13**, 766-769.
3. K. Jiang and W.-B.Cai, *Appl. Catal. B*, 2014, **147**, 185-192.
4. Z.-Y. Shih, C.-H.Wang, G. Xu and H.-T. Chang, *J. Mater. Chem. A*, 2013, **1**, 4773-4778.
5. T. Chierchie and C. Mayer, *J. Electroanal. Chem.*, 1982, **135**, 211-220.
6. T. Bligaard and J. K. Nørskov, *Electrochim. Acta*, 2007, **52**, 5512-5516.
7. S. Hu, L. Scudiero and S. Ha, *Electrochem. Commun.*, 2014, **38**, 107-109.
8. E. Ortiz-Ortega, M.-A. Goulet, J. W. Lee, M. Guerra-Balcázar, N. Arjona, E. Kjeang, J. Ledesma-García and L. G. Arriaga, *Lab Chip*, 2014, **14**, 4596.
9. R. S. Jayashree, L. Gancs, E. R. Choban, A. Primak, D. Natarajan, L. J. Markoski and P. J. A. Kenis, *J. Am. Chem. Soc.*, 2005, **127**, 16758-16759.
10. N. Arjona, A. Palacios, A. Moreno-Zuria, M. Guerra-Balcázar, J. Ledesma-García and L. G. Arriaga, *Chem. Commun.*, 2014, **50**, 8151-8153.
11. A. Dector, F. M. Cuevas-Muñiz, M. Guerra-Balcázar, L. A. Godinez, J. Ledesma-García and L. G. Arriaga, *Int. J. HydrogenEnergy*, 2013, **38**, 12617-12622.